Synthesis of GO supported Fe_2O_3–TiO_2 nanocomposites for enhanced visible-light photocatalytic applications

Journal:	*Dalton Transactions*
Manuscript ID:	DT-ART-08-2015-002983
Article Type:	Paper
Date Submitted by the Author:	02-Aug-2015
Complete List of Authors:	selvam, Clament; Kyungpook National University, Department of Environmental Engineering Jo, Wan; Kyungpook National University, Environmental Engineering

Graphical abstract

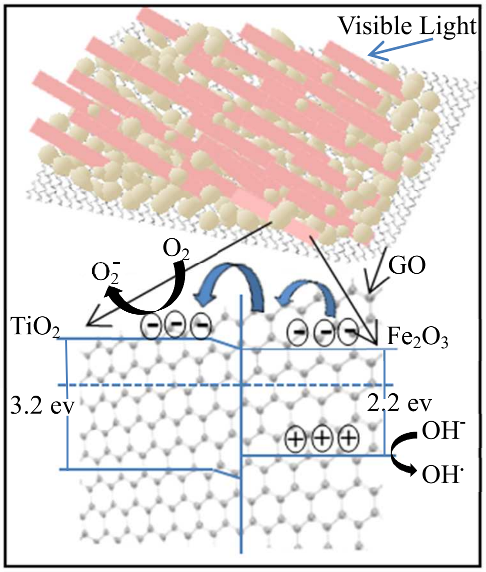

Synthesis of GO supported Fe_2O_3–TiO_2 nanocomposites for enhanced visible-light photocatalytic applications

Wan-Kuen Jo, N. Clament Sagaya Selvam*
Department of Environmental Engineering, Kyungpook National University, Daegu 702-701, South Korea

Abstract

This article reports a novel ternary composite consisting of Fe_2O_3 nanorods, TiO_2 nanoparticles, and graphene oxide (GO) flakes that provide enhanced photocatalytic performance and stability. Fe_2O_3 nanorods grow evenly and embed themselves on the agglomerated TiO_2/GO surface, which facilitated the formation of heterojunction for effective migration of charge carriers at the interface of Fe_2O_3/TiO_2 in the ternary composites. The formation of heterostructured Fe_2O_3–TiO_2/GO composites and the effect of GO addition on the photophysical properties of the composites were systematically investigated using various spectroscopic techniques. The photocatalytic performance of Fe_2O_3 was improved by coupling with TiO_2 in the presence of GO, suggesting uncommon electron transfer from the conduction band of Fe_2O_3 to that of TiO_2 via GO under visible-light irradiation. Improved charge separation in the composite materials compared with those in bare Fe_2O_3 was confirmed by drastic fluorescence quenching and stronger absorption in the visible range. The optimum content of GO in the ternary composite was 1.0 wt%, which exhibited the enhanced photocatalytic activity. The synergistic effect, heterostructured composite and role of GO, as an electron transporter, in the ternary composites account for the enhanced photocatalytic activity.

Keywords: nanorods, heterojunction, fluorescence quenching, ternary composite

---

*Corresponding author. Tel.: +82539506584; fax: +82539506579.

E-mail address: clamentloy@gmail.com

1. Introduction

Solar energy conversion for environmental applications has received much attention in recent years.[1, 2] Heterogeneous photocatalysis has been extensively used for wastewater treatment and air purification.[1-3] Semiconductor metal oxides, in particular, have been widely used as photocatalysts for the decomposition of organic pollutants and air contaminants, because of their high stabilities, redox capacities, low toxicities, and photophysical properties.[4-6] Fe_2O_3 (bandgap~2.0-2.2 eV) is one of the desirable semiconductor material for photocatalytic applications, because of its useful properties, including absorption in the visible range of the solar spectrum, high stability, low cost, and ready availability.[7,8] However, its photocatalytic performance is limited by swift recombination of electron–hole pairs.[9] Many methods have been used to enhance the photocatalytic activity of Fe_2O_3, including surface alteration, metal/nonmetal doping, and coupling with another semiconductor.[10-13] The design of Fe_2O_3-based composites is an efficient strategy for enhancing charge separation. It is therefore highly desirable to couple Fe_2O_3 with a semiconductor that has a lower conduction band (CB) edge to achieve transfer of photoexcited electrons under visible light, to retard charge recombination. However, it has been shown that the charge separation efficiency of Fe_2O_3 can be increased by coupling with $TiO_{2.}$ This suggests unusual electron transfer from the CB of Fe_2O_3 to the CB of TiO_2.[14-20] This electron transfer has been achieved by tuning the structure and band gap of either Fe_2O_3 or TiO_2.[14-20] Luan et al.[21] reported unusual charge transport between Fe_2O_3 and TiO_2 via phosphate bridges under visible light, leading to enhanced charge carrier separation. Recently, activated carbon has been used for charge transport between Fe_2O_3 and a coupled semiconductor.[22, 23] Nevertheless, this composite also suffers from small surface area and low quantum efficiency. Therefore, hybridizing Fe_2O_3 with a suitable support may address this issue, and improve photocatalytic activity. Graphene oxide (GO) has oxygen functional groups, high electron mobility, and high surface area. These properties are beneficial for charge transport and separation, and making it a suitable support.[24] Furthermore, Xie et al.[15] reported that charge separation can be achieved by coupling anatase TiO_2 with Fe_2O_3, and demonstrated that the charge transfer in one-dimensional materials are better than that in zero-dimensional materials. Here, by considering the importance of materials dimension and role of support, we report a novel ternary nanocomposites consisting of one-dimensional Fe_2O_3 nanorods, TiO_2, and GO as a support, for the degradation of methylene blue (MB). The GO acted as an electron transporter, which facilitated charge separation in the ternary composites.

2. Experimental

2.1. Preparation and characterization of photocatalysts

The Fe_2O_3–TiO_2 composite was prepared using a wet-impregnation method. TiO_2 powder (0.5 g) was added to a 1.0 M ethanol solution of $Fe(NO_3)_3 \cdot 9H_2O$ (50 mL). The suspension was vigorously stirred for 12 h, and the solvent was evaporated at 70 °C. The obtained products were washed with ethanol. The samples were calcined at 300 °C for 6 h. Pure Fe_2O_3 was synthesized using the same procedure, without the addition of TiO_2. GO was synthesized using Hummer's method.[25] Graphite powder (5.0 g) was mixed with concentrated H_2SO_4 (120 mL) in an ice bath. $KMnO_4$ (15 g) was added to the suspension under constant stirring, and the mixture was heated at 40 °C for 45 min. Deionized water (250 mL) was added, and the resulting suspension was left to oxidize at room temperature for 30 min. Deionized water (70 mL) and H_2O_2 (15 mL) were slowly added to the suspension, and the suspension was left for 30 min. The resulting yellow suspension was centrifuged at

3000 rpm to obtain the solid product, which was washed with dilute HCl and acetone. Finally, the sample was heated at 400 °C for 2 h to obtain GO powder. The Fe_2O_3–TiO_2/GO ternary nanocomposites were synthesized as follows. A 1.0 M $Fe(NO_3)_3 \cdot 9H_2O$ ethanol solution (50 mL) was slowly added to TiO_2 powder (0.5 g) containing the appropriate amount of GO. The suspension was vigorously stirred for 12 h, and the solvent was evaporated at 70 °C, using a hot plate. The obtained sample was washed thoroughly with ethanol. Then, the solid powder was dried at 70 °C for 3 h and calcined at 300 °C for 6 h. The GO contents were expressed as weight percentages.

The prepared samples were characterized using X-ray diffraction (XRD; Rigaku D/max-2500), X-ray photoelectron spectroscopy (XPS; Quantera SXM), field-emission scanning electron microscopy (FESEM; Hitachi S-4300 FE-SEM), transmission electron microscopy (TEM; Hitachi H-7600 FE-TEM), N_2 adsorption–desorption isotherms, ultraviolet-visible (UV-vis) spectroscopy (Varian CARY 5G), and fluorescence spectroscopy (Varian Cary Eclipse). Photocurrent measurements were performed on an electrochemical analyzer in a standard three-electrode system by using the prepared sample film as the working electrode, platinum (Pt) coil and saturated calomel electrode (SCE) was used as the counter and reference electrode, respectively. Working electrodes of samples were prepared by grounding the sample (200 mg) using mortar and pestle in an ethanol solvent (2 mL) to make slurry. Then the slurry was coated on the indium-tin oxide (ITO) glass by doctor blade method, and calcined at 573 K for 1 h. Na_2SO_4 (0.1 M) aqueous solution was used as the electrolyte. Subsequently photocurrent was measured under visible light irradiation in different on and off irradiation cycles.

2.2. Photocatalytic degradation (PCD)

The photocatalytic performances of the synthesized photocatalysts were evaluated based on the degradation of MB under visible-light illumination (light source: 500 W xenon lamp). The photocatalyst (30 mg) was mixed with MB (100 mL, 10 mg L^{-1}) solution in a beaker. The suspension was stirred for 30 min in the absence of light to attain adsorption–desorption equilibrium. At certain time intervals during the photocatalytic reaction, samples (2 mL) were collected from the reaction vessel, and centrifuged at 10 000 rpm for 30 min to remove the photocatalyst. The concentration of the sampled solution was determined using a UV-vis spectrophotometer. The stability of the photocatalyst was examined after five consecutive cycles. The amount of photocatalyst used in each cycle was 30 mg/100 mL, and the MB concentration was 10 mg L^{-1}. After visible-light irradiation for 150 min, the suspension was centrifuged at 10 000 rpm for 30 min to remove the photocatalyst particles. The photocatalyst was washed with deionized water and dried at 70 °C for 12 h for the next run.

3. Results and discussion

3.1. Structures, morphologies, and surface areas of nanostructured photocatalysts

The XRD patterns of GO, Fe_2O_3, TiO_2, binary composite (Fe_2O_3–TiO_2), and the ternary composites (Fe_2O_3–TiO_2/GO) are shown in Fig. 1. Fig. 1(a) shows diffraction peaks at 2θ =11° and 2θ =43°, corresponding to the (002) and (100) reflections, respectively, of GO[26, 27]. Pure Fe_2O_3 (Fig. 1b) shows diffraction peaks at 2θ = 24.2°, 33.1°, 35.7°, 40.9°, 49.4°, 54.2°, 57.6°, 62.4°, 64.0°, 69.6°, 72.0°, and 75.5°, assigned to the (012), (104), (110), (113), (024), (116), (122), (214), (300), (208), (101), and (220) diffraction planes, respectively (JCPDS, No. 33-0664). The diffraction peaks for TiO_2 (Fig. 1c) also match the standard data

(JPCDS, No. 21-1272). The Fe_2O_3 crystal phase did not change after coupling with TiO_2 (Fig. 1d), but the characteristic TiO_2 diffraction peaks were observed, indicating the formation of a two-phase composite. The diffraction peaks of ternary composites shift slightly toward lower angles on GO addition as shown in Fig. 1(e, f). Furthermore, the intensity of the diffraction peaks decrease and the peaks width broaden as the amount of GO increases, indicating interaction of GO in the ternary composites.

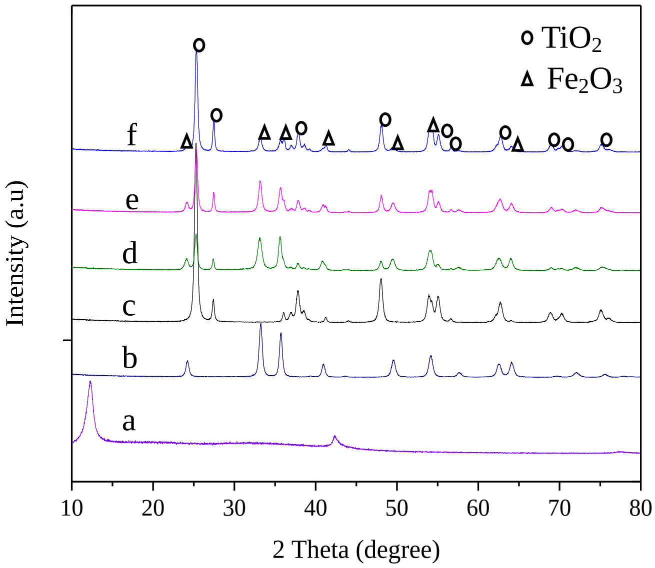

Fig.1 XRD patterns of (a) pure GO, (b) pure Fe_2O_3, (c) pure TiO_2, (d) Fe_2O_3-TiO_2 (e) Fe_2O_3-TiO_2/GO (1.0 %), and (f) Fe_2O_3-TiO_2/GO (10 %)

The surface morphologies of pure materials, the binary composite (Fe_2O_3–TiO_2), and the ternary composite (Fe_2O_3–TiO_2/GO(1%)) were examined using SEM (Fig. 2 and Fig. 3). Fig. 2(a-b) shows the formation of aggregated Fe_2O_3 nanorods. The SEM image of pure TiO_2 (Fig. 2c-d) reveals that the TiO_2 spherical nanoparticles are agglomerated. The SEM image of pure GO (Fig. 2e-f) shows flakes like morphology. In the case of binary composite, Fe_2O_3 nanorods are well grown over the agglomerated TiO_2 surface (Fig. 3a-b), indicating the coupling between Fe_2O_3 and TiO_2. Fig. 3(c-d) shows the

surface morphology of the ternary composite. The images indicate that the composite consists of Fe_2O_3 nanorods on the agglomerated TiO_2/GO surface. The SEM image of ternary composite and the corresponding EDX spectrum from different region (Fig. 3e-f) indicates the formation of hybrid ternary composite. The EDX peaks showed the presence of Fe, Ti, O, and C. This suggests the formation of heterojunctions consist of Fe_2O_3, TiO_2, and GO. TEM analysis was performed to provide further information on the formation of hybrid ternary composite.

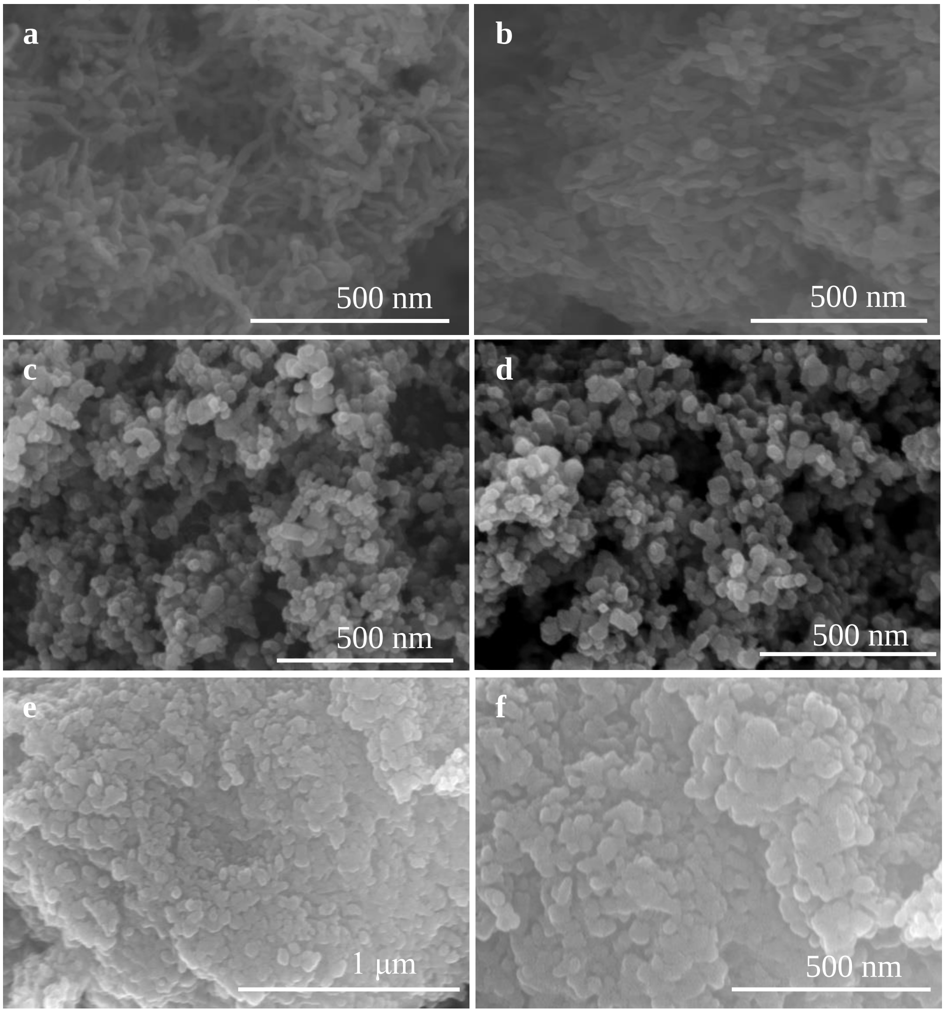

Fig. 2 SEM images of (a, b) pure Fe_2O_3 nanorods, (c, d) pure TiO_2 nanoparticles, (e, f) pure GO flakes

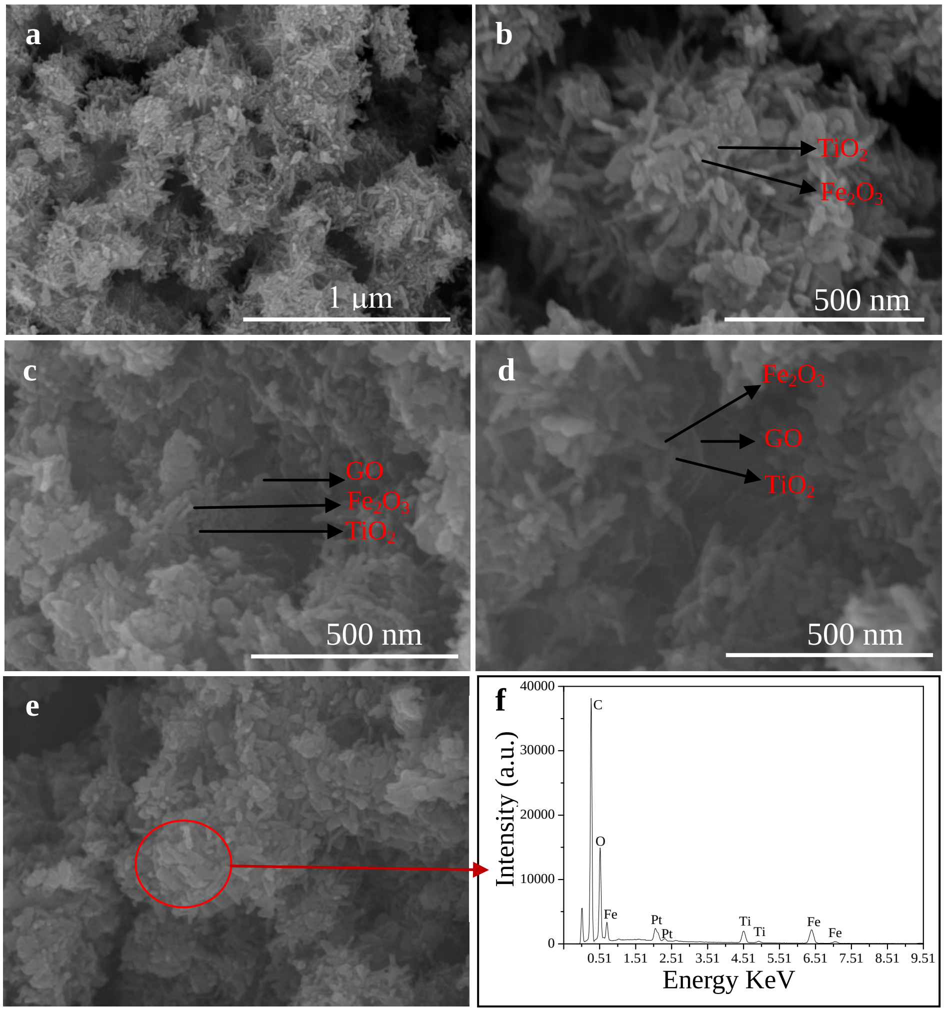

Fig. 3 SEM images of (a, b) binary composite (Fe_2O_3-TiO_2), (c, d) ternary composite (Fe_2O_3-TiO_2/GO(1.0 %)), (e, f) ternary composite and corresponding EDX spectrum

Bright-field TEM image (Fig. 4a) of the ternary hybrid composite clearly shows the presence of Fe_2O_3 nanorods, TiO_2 nanoparticles and GO flakes, indicating the stacking of all components. Chemical analysis of the hybrid was carried out using high angle annular dark-field (HAADF) scanning transmission electron microscopy (STEM) with EDX elemental mapping. Fig. 4(b) presents a HAADF-STEM image of the hybrid. The elemental maps of the constituting elements Fe, O, Ti, and C (Fig. 4c-f) clearly demonstrate a well-defined compositional profile of the ternary hybrid, suggesting that the hybrid is a uniform mixture of both Fe_2O_3 and TiO_2, along with GO support. Further chemical analysis of the hybrid (HAADF-STEM and EDX elemental maps) from different region confirms the formation of ternary hybrid composite (supporting file S1).

Magnified high resolution TEM image (Fig. 5a-d) of the ternary hybrid composite reveals the presence of stacked Fe_2O_3 nanorod, TiO_2 nanoparticle and GO flakes. The diffused rings in the ED pattern (shown as inset in Fig 5c) could be indexed to 101 and 012 planes of TiO_2 and Fe_2O_3 respectively. Lattice fringes in HRTEM image (Fig.5c) of the hybrid could be attributed to lattice spacing of TiO_2 (0.35 nm) and Fe_2O_3 (0.37 nm). Uniform composition was further confirmed by EDX analysis from several regions of the hybrid as discussed below.

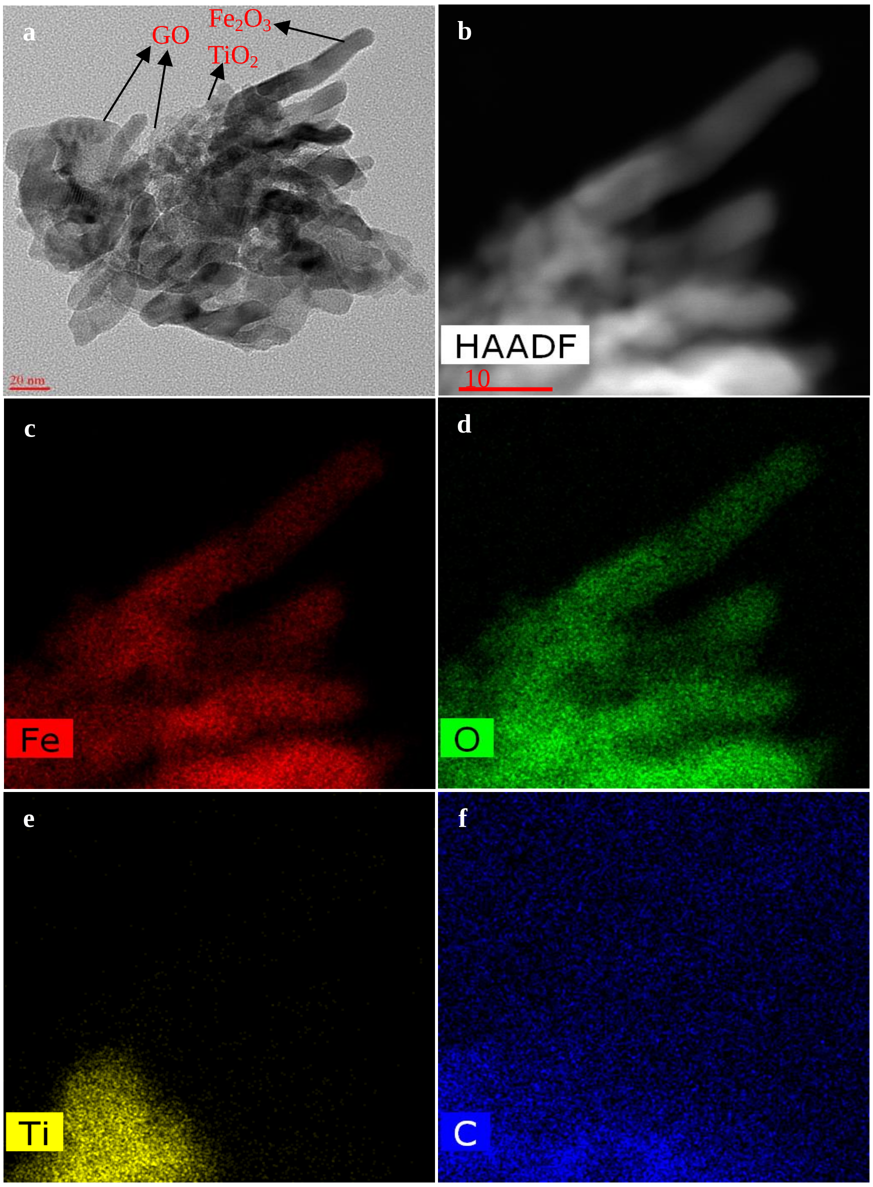

Fig. 4 TEM images of (a) ternary composite (Fe_2O_3-TiO_2/GO(1.0 %), (b)corresponding HAADF STEM image, and the spatially resolved Fe (c), O (d), Ti (e), and C (f) elemental maps of ternary composite

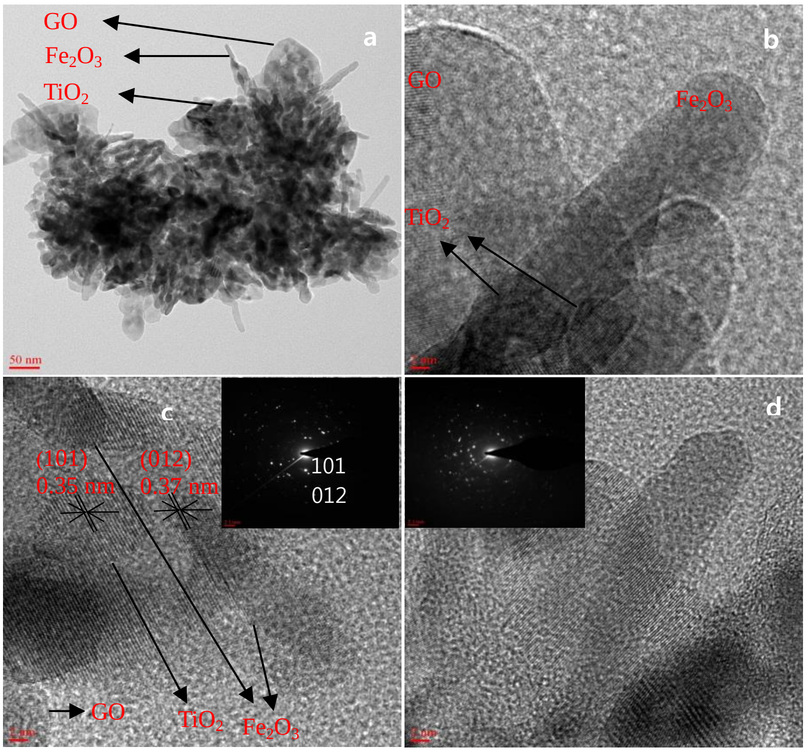

Fig. 5 HRTEM images of ternary composite (Fe_2O_3-TiO_2/GO(1.0 %) from different region (a-d)

The composition of ternary hybrid composite was determined from different regions using energy-dispersive X-ray spectroscopy (Fig.6). The corresponding EDX peaks showed the presence of Fe, Ti, O, and C. The absence of any other peaks suggests that the composite is free of impurities.

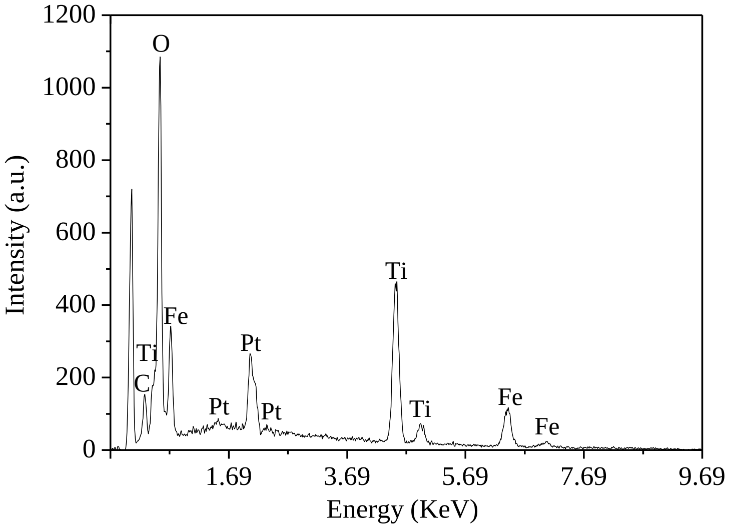

Fig.6 EDX spectrum of ternary composite (Fe_2O_3-TiO_2/GO (1.0 %))

The specific surface areas of the prepared photocatalysts were evaluated using nitrogen adsorption–desorption analysis (Fig.7). Surface areas, pore volumes and mean pore diameters of the synthesized photocatalysts are given in Table 1. The specific surface area of pure Fe_2O_3, TiO_2 and GO are 40.0 m^2g^{-1}, 46.2 m^2g^{-1}, and 90.7 m^2g^{-1} respectively. The surface area of the binary composite (Fe_2O_3-TiO_2) is 61.9 $m^2g,^{-1}$. The surface area of the ternary composites increases with the increase of GO, and are relatively higher than those of pure samples (Table 1). The higher specific surface areas of the ternary composites are due to the presence of the GO support. This improves the reactant adsorption, and provides more reaction sites for effective photocatalysis.

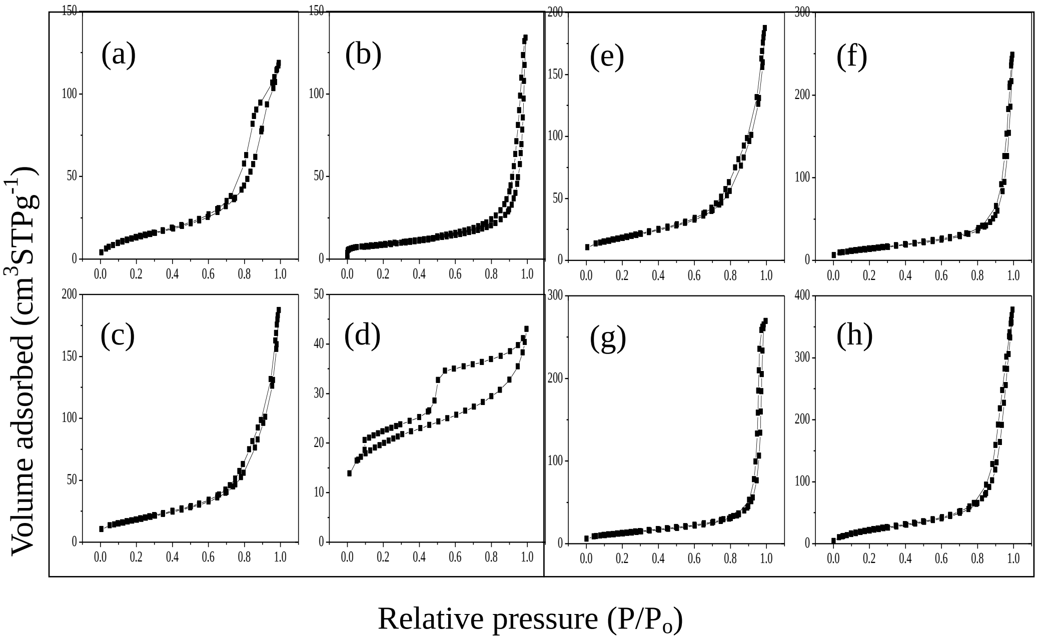

Fig.7 N_2 adsorption /desorption isotherms of (a) pure Fe_2O_3, (b) pure TiO_2, (c) binary composite (Fe_2O_3-TiO_2), (d) pure GO, (e) ternary composite (Fe_2O_3-TiO_2/GO (0.5 %)), (f) ternary composite (Fe_2O_3-TiO_2/GO (1.0 %)), (g) ternary composite (Fe_2O_3-TiO_2/GO (5 %)), (h) ternary composite (Fe_2O_3-TiO_2/GO (10 %))

Table1 Surface area, pore volumes and mean pore diameters of the synthesized photocatalyts

Photocatalysts	Surface area (m^2/g)	Pore volume (cm^3/g)	Mean pore diameter (nm)
Pure Fe_2O_3	40.0	0.182	13.78
Pure TiO_2	46.2	0.206	26.0
Fe_2O_3-TiO_2	61.9	0.286	17.10
Pure GO	90.7	0.064	3.63
(Fe_2O_3-TiO_2/GO (0.5 %)	76.8	0.296	25.83
(Fe_2O_3-TiO_2/GO (1.0 %)	78.1	0.356	27.6
(Fe_2O_3-TiO_2/GO (5 %)	81.3	0.410	35.52
(Fe_2O_3-TiO_2/GO (10 %)	88.0	0.558	25.30

3.2. XPS analysis of nanostructured photocatalysts

The Fe2p, O1s, Ti2p, and C1s XP spectra of ternary composite (Fe_2O_3–TiO_2/GO) are shown in Fig. 8(a–d), respectively. The Fe2p spectrum (Fig. 8a) shows two peaks, at 711.1 and 725.8 eV, ascribed to $Fe2p_{3/2}$ and $Fe2p_{1/2}$, respectively; these are the typical binding energies of Fe^{3+} in Fe_2O_3.[14, 21] Meanwhile, the fitted Fe $2p_{3/2}$ peak (deconvoluted) shows an additional peak at 724.0 eV, which is assigned to a Fe^{2+} in Fe_2O_3**[28]**. Thus, Fe_2O_3 has an inverse spinel structure which has both Fe^{3+} and Fe^{2+} in its lattice**[28]**. The shakeup satellite peak present at 719.1eV, is characteristic for Fe^{3+} ions in α-Fe_2O_3 **[28]**. The peak observed at 530.0 eV in the O1s spectrum (Fig. 8b) is ascribed to oxygen atoms bound to Fe–O and Ti–O in the ternary composite.[21] The additional peak at 531.8 eV is attributed to surface hydroxyl group**[28]**. The appearance of Ti2p doublets at 458.8 and at 464.5 eV can be ascribed to the presence of Ti^{4+} (TiO_2) in the ternary composite material[14] as shown in Fig. 8(c). The C1s peak can be deconvoluted into three main components corresponding to carbon atoms in different functional groups (Fig. 8d). The non-oxygenated ring C (284.8 eV), the C in C–O bonds (286.4 eV), and the carbonyl C (C=O, 288.7 eV) of GO**[29]**. The XP spectra show the presence of Fe, Ti, O, and C on the composite surface, and confirm heterojunction formation. Moreover, the carbon–oxygen species in GO could serve as active sites for interaction between TiO_2 and Fe_2O_3. This is beneficial for the formation of heterojunctions, which facilitate the charge transport and separation. [28-32]

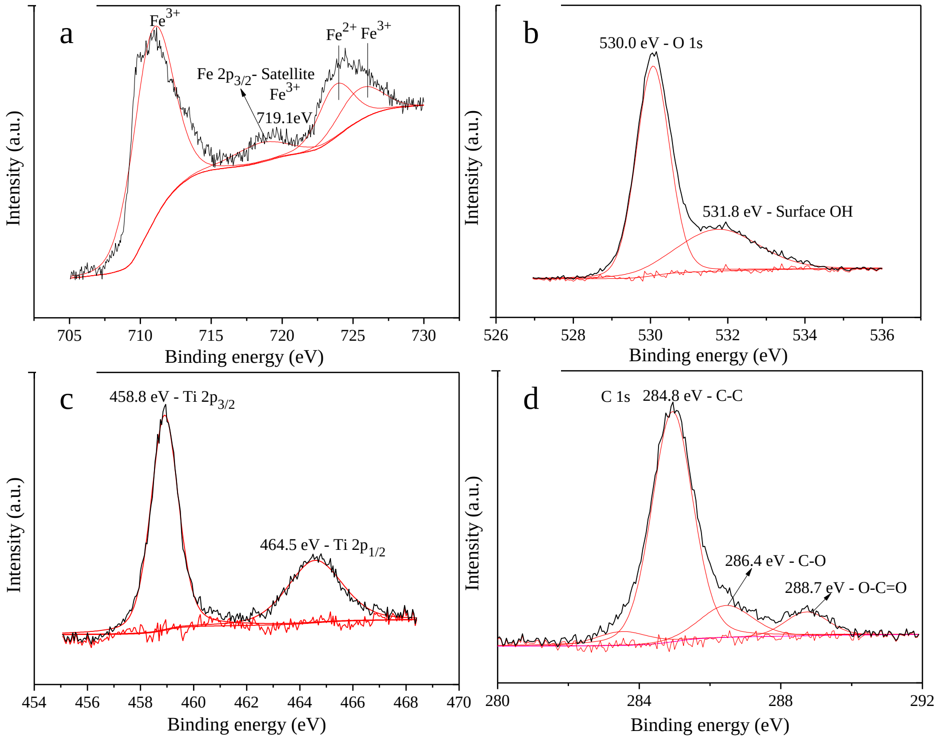

Fig.8 XPS data of (a) Fe2p, (b) O1s, (c) Ti2p, and (d) C 1s for the ternary composite (Fe_2O_3-TiO_2/GO (1.0 %)) (Note: black line - raw data and red line - deconvoluted fitting)

3.3. UV-vis diffuse reflectance spectroscopy (DRS) analysis of nanostructured photocatalysts

Fig. 9(A) and (B) shows the Normalized UV-vis DRS spectra of the prepared photocatalysts. Pure TiO_2 has an absorption edge at 390 nm (3.13 eV), which can be attributed to the band gap of TiO_2. Pure Fe_2O_3 has a characteristic band gap absorption edge at 580 nm (2.06 eV).[19, 22] As shown in Fig. 9(A), the absorption edge of the binary composite (Fe_2O_3–TiO_2) shifts to the visible range and has a high absorption intensity than Fe_2O_3 (as a result of electronic interactions between Fe_2O_3 and TiO_2), indicating effective surface hybridization between these components[17, 19, 22]. The absorption edge of the ternary composite samples (Fe_2O_3–TiO_2/GO) increases with increasing GO loading, reaches a maximum absorption (468 nm, 2.64 eV) at 1.0% GO, and then decreases on further GO addition to 10% (462, 2.68 eV). The addition of GO leads to a continuous absorption band in the range 400–800 nm (unlike bare TiO_2 and Fe_2O_3), suggesting Ti–O–C and Fe–O–C interactions in the ternary composite[33–35]. This band gap narrowing is attributed to delocalization of surface charges as a result of GO interactions in the ternary composite. This observation has been previously reported for semiconductors coupled with GO[33–35]. The decreased absorption above optimal loading of GO (10%) may be due to the fact that such treatment may shield the Fe_2O_3, and preventing absorption as reported.[17]

The absorption features of physical mixtures (Fe_2O_3/TiO_2/GO), prepared by mechanical grinding, were investigated (Fig. 9B) for comparison. The Fe_2O_3:TiO_2:GO weight ratios in the physical mixtures were the same as those in the synthesized ternary composite materials. The absorption spectra of the physical mixtures (Fig. 9B) show two distinct humps (absorption edges), at 400 and 600 nm, indicating the band gap absorption edges of the individual materials, i.e., TiO_2 and Fe_2O_3, respectively. The addition of GO in the physical mixture did not shift the absorption edges in the visible range or narrow the band gap (red shift) as observed for the composite materials (Fig. 9A), indicating that Fe_2O_3, TiO_2, and GO are present as individual components in physical mixture. The significant continuous absorption across the whole spectral range of the synthesized ternary composites (Fig. 9A) suggests the formation of a combined heterojunction, which enhances absorbance in the visible region. This is beneficial for the maximum utilization of solar light for the photocatalysis.

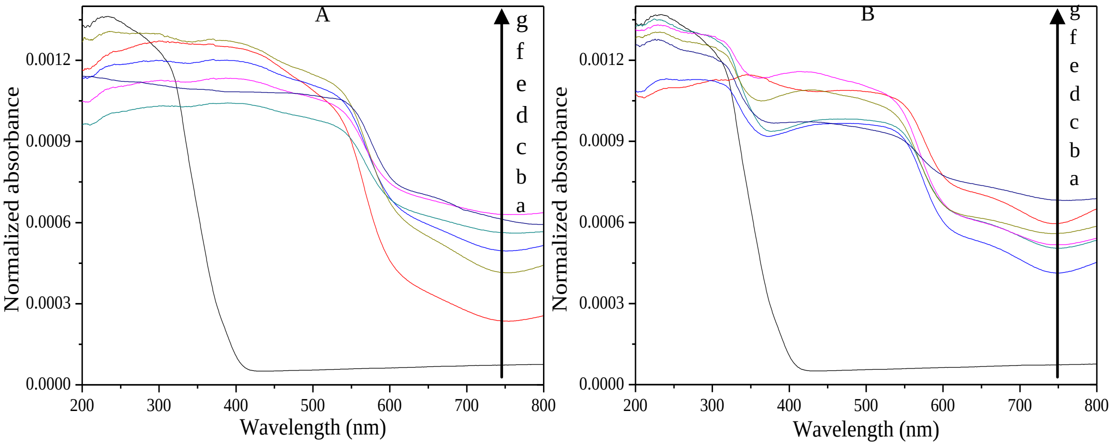

Fig.9 Normalized UV-Vis DRS spectra of photocatalysts (A) ((a) TiO_2, (b) Fe_2O_3, (c) Fe_2O_3-TiO_2, (d) Fe_2O_3-TiO_2/GO(0.5%), (e) Fe_2O_3-TiO_2/GO(5%), (f) Fe_2O_3-TiO_2/GO(1%), (g)Fe_2O_3-TiO_2/GO(10%)), and (B) Physical mixtures ((a) TiO_2, (b) Fe_2O_3, (c) Fe_2O_3-TiO_2, (d) Fe_2O_3-TiO_2/GO(0.5%), (e) Fe_2O_3-TiO_2/GO(5%), (f) Fe_2O_3-TiO_2/GO(1%), (g) Fe_2O_3-TiO_2/GO(10%))

3.4. Photocatalytic performances of nanostructured photocatalysts

The results for the PCD of MB are shown in Figs. 10 and 11. Photolysis was not observed during visible-light irradiation for 150 min, indicating that MB is stable under light illumination. The PCD results fitted pseudo-first-order kinetics, as shown in Fig. 10. The value of the rate constant k was calculated from $\ln(C/C_0) = kt$, where k represents the rate constant (min^{-1}), C_0 and C are the initial concentration and at time‘t’ of the MB, respectively. The calculated rate constant *k* is given as the inset of Fig.10. The PCD efficiency of pure TiO_2 was 17.0 %, with a rate constant *k* of 0.0015 min^{-1}, after 120 min of irradiation. The PCD efficiency of pure Fe_2O_3 was 30.0%, with a rate constant *k* of 0.0029 min^{-1} after 120 min of irradiation. This is considerably higher than that of pure TiO_2 as it absorbs more visible light. The PCD efficiency and degradation rate constant (*k*) of binary composite (In the present study, weight ratio of Fe_2O_3:TiO_2–50%:50%) were 40.0% and 0.0042 min^{-1}, respectively, after 120 min of irradiation, as shown in Fig. 10. Meanwhile, the PCD efficiency of binary composite (Fe_2O_3–TiO_2) was 70.0% after 150 min of irradiation (Fig.11). This considerable enhancement of the PCD performance can be attributed to heterojunction formation and subsequent transfer of charge carriers at the Fe_2O_3–TiO_2 interfaces in the binary composite.[14–19] Notably, the PCD performance of ternary composites (Fe_2O_3/TiO_2/GO) increased significantly with increasing GO content to 1.0%, and then decreased slightly on further GO loading to 10%, as shown in Fig. 10 and 11. The ternary composite (Fe_2O_3–TiO_2/GO (1.0%)) showed the best photocatalytic performance, with a PCD efficiency of 76.0% (*k*=0.011) after 120 min of light irradiation, as shown in Fig. 10. Meanwhile, it exhibited the maximum PCD efficiency of 98.0% after 150 min of light irradiation (Fig. 11). The inset in Fig. 11 shows the UV-vis spectrum of MB degradation using ternary composite (Fe_2O_3–TiO_2/GO (1.0%)), indicating complete degradation within 150 min. The GO loading (10%), above the optimum content, in the ternary composite decrease the photocatalytic activity. This may be due to the fact that excess GO loading reduces the light absorption in the suspension during the photocatalytic reaction as it increases the sample opacity.[36]

For the purpose of comparison, the concentration of TiO_2 has been varied (10%-70%) in the ternary composite with the constant content of GO (1%). The PCD performance increase as TiO_2 content increase, and reaches maximum (PCD=99.0%) at 50% TiO_2 content (supporting file S2). However, increasing TiO_2 content above the optimal level (70%) decreased the PCD efficiency (supporting file S2). The decreased

performance above optimal loading may be due to the fact that such treatment may shield the Fe_2O_3, preventing absorption of light irradiated during PCD reaction, as reported for the similar photocatalytic systems[37]. Moreover, it is suggested that the present ternary composite is more efficient than the reported photocatalytic systems in degradation of MB. The photocatalytic activity of the present system was compared with the similar photocatalytic system reported, and the results were tabulated in Table 2. Table 2 indicates that either higher amount of photocatalyst or more reaction time has been used for the degradation of MB. However in our photocatalytic system, we have used less amount of photocatalyst for the degradation of MB as given in Table 2. The key features for the enhanced photocatalytic performance of ternary composite were discussed in section 3.5. The stability of the ternary composite was evaluated to determine whether it would be suitable for practical applications. No obvious decrease in photocatalytic activity was observed after five cycles, indicating that the composite material retained its stability. Moreover, the MB adsorption performance of ternary composite showed a removal efficiency of 32.5% over a period of 150 min due to the presence of GO. **The visible-light photocatalytic activity of ternary composite (Fe_2O_3-TiO_2/GO1%) has also been evaluated using 4-chlorophenol (colorless molecules), and thereby excluded the possibility of dye sensitization effect (Fig.12). Notably, the ternary composite showed superior photocatalytic performance than the binary and bare photocatalysts, with a PCD efficiency of 99.0% after 210 min of light irradiation (Fig.12). Fig. 13 shows the UV-vis profile for this reaction, confirming the degradation within this time frame.**

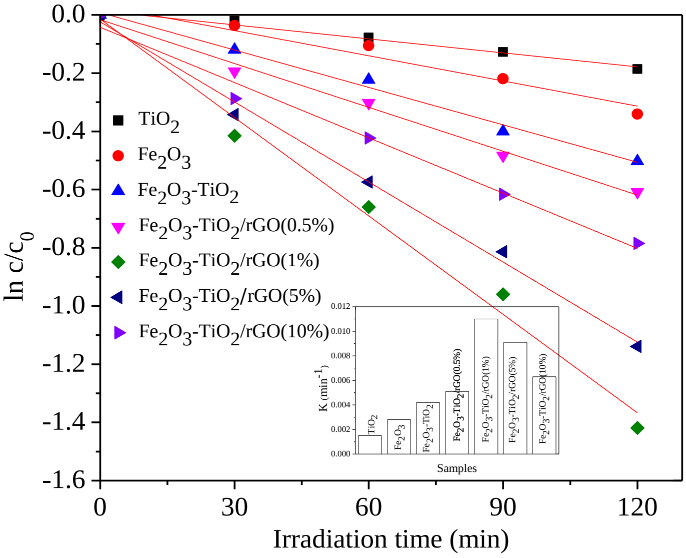

Fig.10 Kinetic PCD plot for MB using the prepared photocatalysts after 120 min of visible light illumination

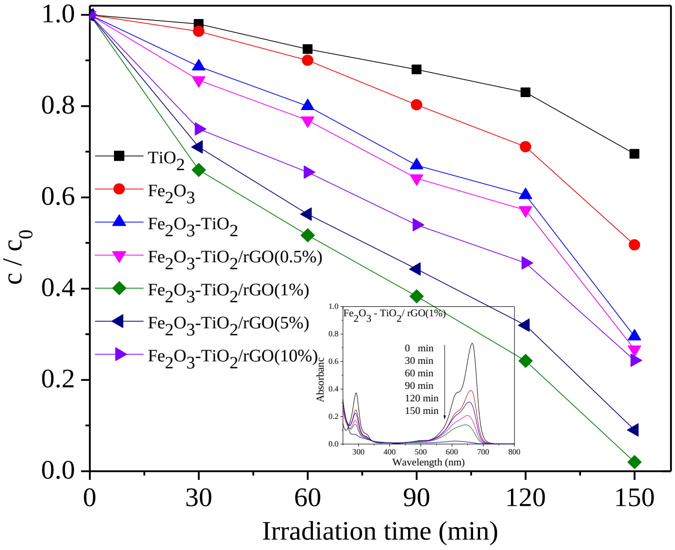

Fig.11 PCD of MB using the prepared photocatalysts after 150 min of visible light illumination

Table 2 Comparison of photocatalytic performance with literature

S. No	Catalyst	Concentration (mg/L) and Volume (mL) of pollutants	Catalyst amount (mg)	Degradation (%)	Light source	Illumination time (min)	Ref.
1	Fe_2O_3-TiO_2 composite	25 and 80 Methylene blue	200	88	Iodine tungsten (300 W)	300	40
2	Fe_2O_3-TiO_2 composite	3 and 100 Methylene blue	100	~95	Hg lamp	60	41
3	Fe_2O_3-TiO_2 composite	20 and 20 Orange II	50	~55	Xe lamp (500 W)	180	19
4	Fe_2O_3-TiO_2 composite	10 and 50 Rhodamine b	5	~60	Xe lamp (350 W)	300	17
5	Fe_2O_3–TiO_2 composite	50 and 100 2,4-dichlorophenoxyacetic acid	10	~ 100	Xe lamp (300 W)	150	14
6	TiO_2-Fe_2O_3 composite	10 and 60 Phenol	200	~17	Xe lamp (150 W)	60	15
7	Fe_2O_3-TiO_2 composite	100 and 100 4-chlorophenol	100	~100	Sunlight	180	42
8	Fe_2O_3-TiO_2 composite	10 and 100 Methylene blue	30	70	Xe lamp (500 W)	150	Present study
9	Fe_2O_3-TiO_2/GO composite	10 and 100 Methylene blue	30	98	Xe lamp (500 W)	150	Present study

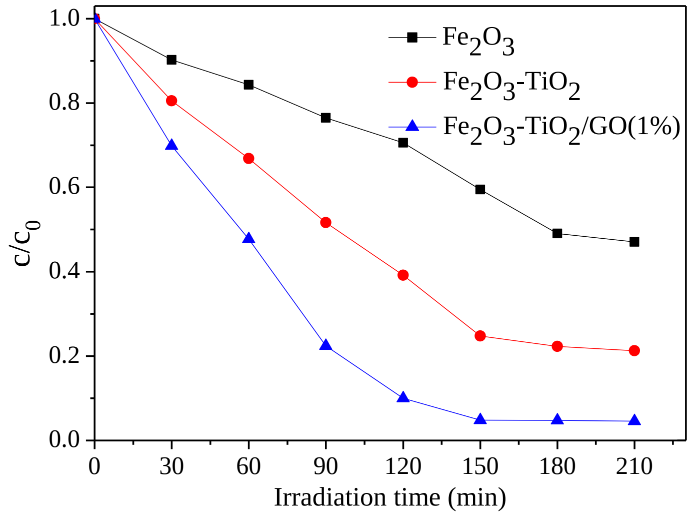

Fig.12 PCD of 4-chlorophenol using the prepared photocatalysts after 210 min of visible light illumination (Experimental conditions: 4-CP concentration = 50 mg/L, photocatalyst = 30 mg/100 mL, initial pH of suspension = 6–6.5 (natural pH).

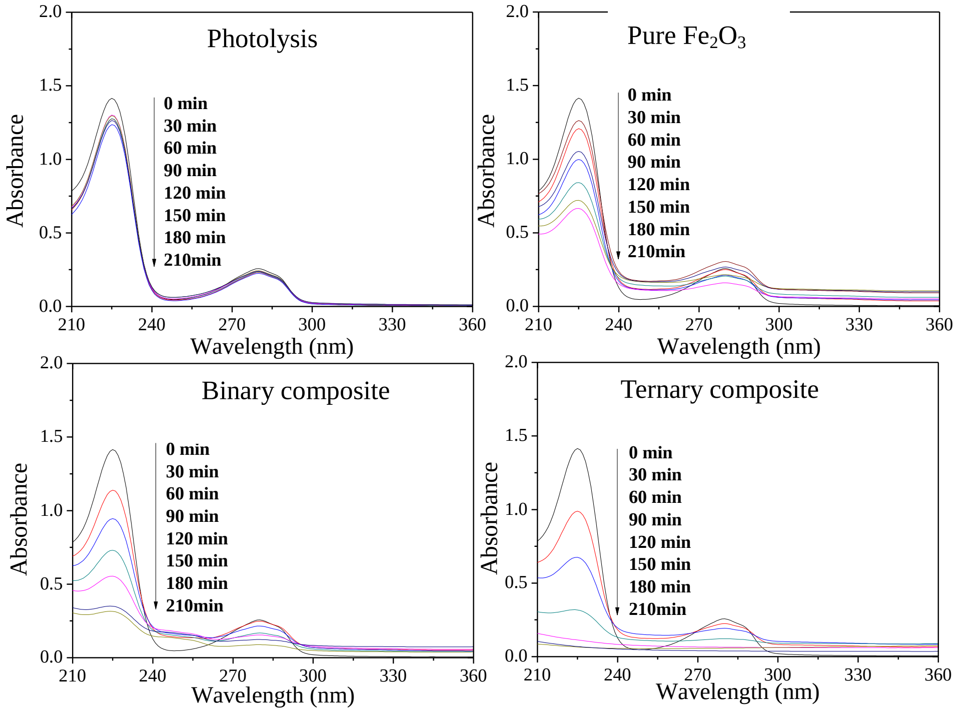

Fig.13 UV-visible degradation spectra of 4-chlorophenol using the prepared photocatalysts (Experimental conditions: 4-CP concentration = 50 mg/L, photocatalyst = 30 mg/100 mL, initial pH of suspension = 6–6.5 (natural pH).

3.5. Reasons for enhanced PCD of heterostructured ternary nanocomposites

The enhanced photocatalytic performance of ternary composites (Fe_2O_3/TiO_2/GO) was ascribed to the following key features: the Fe_2O_3 morphology (one-dimensional nanorods), heterojunction of the ternary composite, high surface area, strong absorption in the visible region, band bending of TiO_2 for electron transfer, and enhanced charge separation efficiency of the ternary composite. These features are discussed below.

Pradhan et al.[38] reported that the electron-transporting ability of one-dimensional Fe_2O_3 nanorods was superior to those of other morphological forms of Fe_2O_3. In the case of ternary composite in the present study, the one-dimensional Fe_2O_3 nanorods improved the electron mobility in the (001) direction of the nanorods, and suppressing electron–hole recombination. The heterojunction nature of the ternary composite is responsible for the improved migration of charge carriers at the interface between two oxide semiconductors in the present study as reported for similar Fe_2O_3/TiO_2 composites.[17] The surface area of a catalyst generally plays an important role in the PCD performance. The number of active sites on the catalyst surface increases with increasing surface area, which enables more reactant molecules to be degraded.[15, 39] The surface areas of the prepared photocatalysts follow the order of pure photocatalyst < binary composite < ternary composite, as shown in Table 1. The ternary composite therefore accommodates more reactant molecules as it has the highest surface area, resulting in greater PCD. The ternary composite samples have stronger absorptions (narrow band gap) in the visible range than do the other samples prepared in this study, as discussed in section 3.3. This extended and strong absorption leads to the formation of more photoinduced charge carriers under visible-light irradiation, facilitating the degradation of more reactant molecules.[39] The downward band bendings of the CB and valence band (VB) of TiO_2 at the heterojunction interface are presumed to occur, and are attributed to uncommon electron transfer from the CB of Fe_2O_3 to the CB of TiO_2, as previously reported.[19] This suppresses electron–hole recombination and improves the degradation performance of the ternary composite. Generally, photocatalytic reactions are more dependent on the rate of electron–hole recombination than on the other factors discussed above. Therefore, the rate of electron–hole recombination was determined from the photoluminescence (PL) emission intensity. The PL spectra of the prepared photocatalysts are shown in Fig. 14. The PL spectrum of pure Fe_2O_3 has a peak at 580 nm, which is attributed to electron–hole pair recombination. The intensity of the peak at 580 nm for the binary composite (Fe_2O_3–TiO_2) is lower, which indicates that charge carrier recombination is lower in the binary composite than in pure Fe_2O_3. The ternary composite samples (Fe_2O_3–TiO_2/GO), in particular, show very weak emission at 580 nm, indicating high charge separation efficiency. The PL results therefore confirm the importance of heterojunction nature of ternary composite in retarding electron–hole recombination for the enhanced PCD performance.

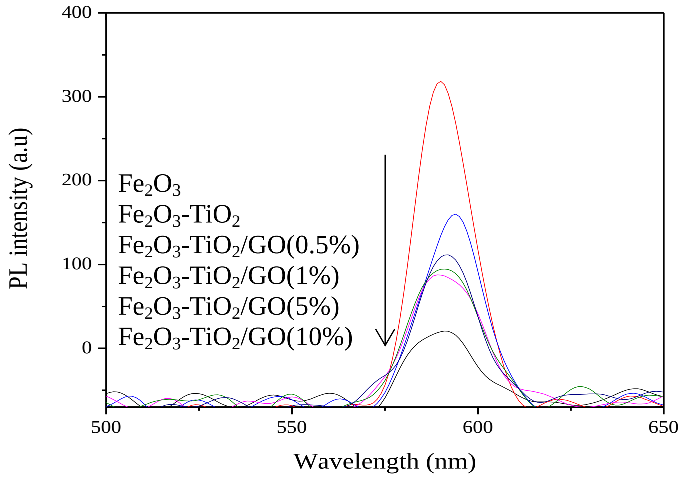

Fig.14 PL spectra of prepared photocatalysts

A possible synergistic mechanism in the heterostructured ternary composite is shown in Scheme 1. Pure Fe_2O_3 absorbs visible light, and electrons are transferred from the VB to the CB, whereas TiO_2 cannot absorb visible light and be excited to form electron–hole pairs. However, in the case of the binary composites, the Fe_2O_3 nanorods coupled on TiO_2 surface lead to band bending of TiO_2 as a result of intimate heterojunction (built-in electric field) formation. This promotes transfer of electrons from the CB of Fe_2O_3 to the CB of TiO_2, thereby increasing the charge separation efficiency[17]. In the presence of GO in the ternary composite, the photoinduced electrons in the CB of Fe_2O_3 migrate to the LUMO of GO (acting as an electron conduction bridge), and are transferred to the CB of TiO_2, thereby reducing charge carrier recombination. Charge carrier separation is therefore achieved in ternary composite. The formed charge carriers subsequently migrate to the surface of the ternary composite, and produce hydroxyl and superoxide radicals with water and dissolved oxygen, respectively, which can then proceed to oxidize MB.[17]

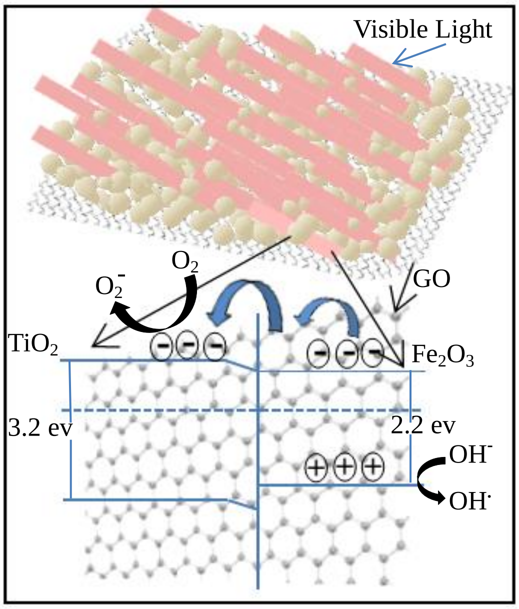

Scheme 1 PCD mechanism of heterostructured ternary composite (Fe_2O_3-TiO_2/GO(1%))

To further prove the efficient separation of photo-induced electrons, and the electron transfer path way in the ternary composite, photocurrent measurements of prepared photocatalysts were carried out in several on-off intermittent irradiation cycles, and the results were shown in Fig. 15. The results revealed that the ternary composite has higher photocurrent response than the other photocatalysts. Notably, Fe_2O_3-GO(1%) showed higher photocurrent response than the binary composite (Fe_2O_3-TiO_2). Therefore, in the case of the ternary composite, photoinduced electrons in the CB of Fe_2O_3 migrate to GO (acting as an electron conduction bridge) faster, and are subsequently transferred to the CB of TiO_2. This reduces the electron/hole pair recombination and enhances the PCD efficiency.

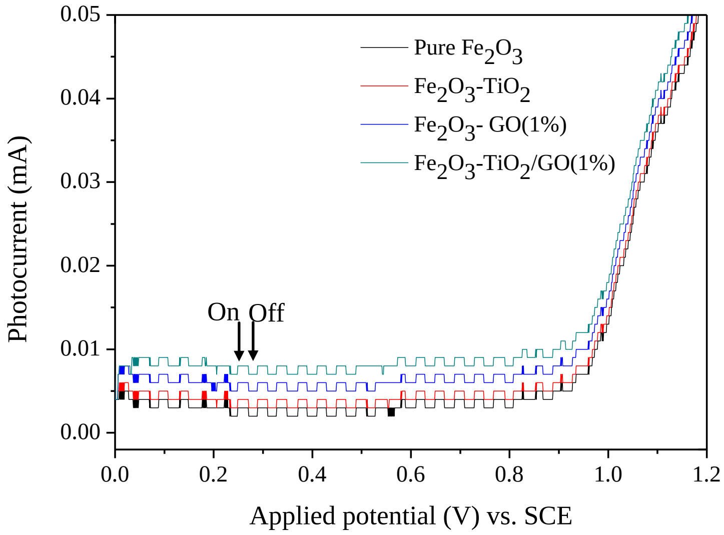

Fig.15 Chopping visible-light photocurrent–voltage curves of photocatalysts in 0.1 M Na_2SO_4 aqueous solution

4. Conclusion

In summary, a novel nanocomposites consisting of Fe_2O_3, TiO_2, and GO, were synthesized using a facile method. The prepared ternary composites exhibited enhanced photocatalytic performance. The GO supported Fe_2O_3–TiO_2 composites showed intimate heterojunction formation, which facilitated unusual electron transfer from the CB of Fe_2O_3 to the CB of TiO_2. UV-vis absorption analysis showed that the ternary composite had continuous and extended visible-range absorption, unlike physical mixtures. The observed suppression of electron–hole recombination in the ternary composite was confirmed by strong florescence quenching in the PL spectra. In addition, the GO support lent the ternary composite superior photocatalytic activity, specifically with respect to increased surface area for MB adsorption, enhanced visible light absorption, and improved charge transportation and separation. These properties make this ternary composite a promising material for energy and environmental applications utilizing visible light.

Acknowledgments

This work was supported by the National Research Foundation of Korea (NRF) grant funded by the Korean government (MEST) (2011-0027916). The authors thank Mr. Joon Yeob Lee and Dr. Seung-Ho Shin for their valuable support.

References

[1] P. Luan, M. Xie, D. Liu, X. Fu, L. Jing, *Scientific reports*, 2014, **4**, 6180.

[2] X. B. Chen, S. H. Shen, L. J. Guo, S. S. Mao, *Chem. Rev*., 2010, **110**, 6503-6570.

[3] F. Amano, K. Nogami, B. Ohtani, *J. Phys. Chem. C*, 2009, **113**,1536-1542.

[4] P. V. Kamat, *J. Phys. Chem. C*, 2007, **111**, 2834-2860.

[5] S. Dong, J. Feng, M. Fan, Y. Pi, L. Hu, X. Han, M. Liu, J. Sun, J. Sun, *RSC Adv*., 2015, **5**, 14610-14630.

[6] K. Rajeshwara, M. E. Osugi, W. Chanmanee, C. R. Chenthamarakshan, M. V. B. Zanoni, P. Kajitvichyanukul, R. Krishnan-Ayer, *J. Photochem. Photobiol. C*, 2008, **9**,171-192.

[7] D. K. Zhong, J. Sun, H. Inumaru, D. R. Gamelin, *J. Am. Chem. Soc*., 2009, **131**, 6086-6087.

[8] Y. J. Lin, G. B.Yuan, S. Sheehan, S. Zhou, D. W. Wang, *Energy Environ. Sci*., 2011, **4** 4862-4869.

[9] R. Franking, L. Li, M. A. Lukowski, F. Meng, Y. Tan, R. J. Hamers, S. Jin, *Energy Environ. Sci*., 2013, **6**, 500-512.

[10] S. D. Tilley, M. Cornuz, K. Sivula, M. Gratzel, *Angew.Chem. Int. Ed*., 2010, **49**, 6405-6408.

[11] J. Lian , X. Duan , J. Ma, P. Peng , T. Kim, W. Zheng, *ACS Nano*, 2009, **11**, 3749-3761.

[12] I. Cesar, A. Kay, J. A. G. Martinez, M. Gratzel, *J. Am. Chem. Soc*., 2006, **128**, 4582-4583.

[13] D. K. Zhong, M. Cornuz, K. Sivula, M. Gratzel, D. R. Gamelin, *Energy Environ. Sci*. 2011, **4**, 1759-1764.

[14] S. J. A. Moniz, S. A. Shevlin, X. An, Z. X. Guo, J. Tang, *Chem. Eur. J*., 2014, **20**, 15571 -15579.

[15] M. Xie, Q. Meng, P. Luan, Y. Feng, L. Jing, *RSC Adv*., 2014, **4**, 52053-52059.

[16] T. Madrakian, A. Afkhami, R. Haryani, M. Ahmadi, *RSC Adv*., 2014, **4**, 44841-44847.

[17] Y. Xia, L.Yin, *Phys. Chem. Chem. Phys*., 2013, **15**, 18627-18634.

[18] K. E. deKrafft, C. Wang, W. Lin, *Adv. Mater*., 2012, **24**, 2014-2018.

[19] L. Peng, T. Xie, Y. Lu, H. Fan, D.Wang, *Phys. Chem. Chem. Phys*., 2010, **12**, 8033-8041.

[20] W. Wu, S. Zhang, X. Xiao, J. Zhou, F. Ren, L. Sun, C. Z. Jiang, *ACS Appl. Mater. Interfaces*, 2012, **4**, 3602-3609.

[21] P. Luan, M. Xie, X. Fu, Y. Qu, X. Sun, L. Jing, *Phys. Chem. Chem. Phys*., 2015, **17**, 5043-5050.

[22] B. A. bi-Feiz, S. Aber, M. Sheydaei, *RSC Adv*., 2015, **5**, 19368-19378.

[23] N. Yusoff, S. Vijay Kumar, A. Pandikumar , N. M. Huanga, , A. R. Marlindaa , M. N. Anamta, *Ceram. Inter*., 2015, **41**, 5117-5128.

[24] L. Zhang, L. Du, X. Yu, S.Tan, X. Cai, P. Yang, Y. Gu, W. Mai, *ACS Appl. Mater. Interfaces*, 2014, **6**, 3623-3629.

[25] W. Hummers, R. Offeman, Preparation of graphite oxide, *J. Am. Chem. Soc*.,1958, **80**, 1339-1339.

[26] Y. Zhao, X. Song, Q. Song, Z.Yin, *CrystEngComm*, 2012, 14, 6710–6719.

[27] H. Feng, Y. Li, J. Li, *RSC Advances*, 2012, **2**, 6988–6993.

[28] R. Suresh, K. Giribabu, R. Manigandan, A. Stephen, V. Narayanan, *RSC Adv.*, 2014, **4**, 17146-17155

[29] T. T. Tung, M. Castro, T. Y. Kim, K. S. Suh, J.F. Feller, *J. Mater. Chem*., 2012, **22**, 21754–21766.

[30] C.Y. Cao, J. Qu, W.S. Yan, J. F. Zhu, Z.Y. Wu, W.G. Song, *Langmuir,* 2012, **28**, 4573-4579.

[31] G. Cheng, M. S. Akhtar, O.B. Yang, F. J. Stadler, *ACS Appl. Mater. Interfaces*, 2013, **5**, 6635-6642.

[32] C. Chen, W. Cai, M. Long, B. Zhou, Y. Wu, D. Wu, Y. Feng, *ACS Nano*, 2010, **11**, 6425-6432.

[33] S. Sakthivel, H. Kisch, *Angew. Chem. Int. Ed*., 2003, 42, 4908-4911.

[34] Y. Jiang, W. N. Wang, P. Biswas, J. D. Fortner, *ACS Appl. Mater. Interfaces,* 2014, **6**, 11766-11774.

[35]Y. Hou, F. Zuo, A. Dagg, P. Feng, *Nano Lett*., 2012, **12**, 6464-6473.

[36] Y. Hou, A. B. Laursen, J. Zhang, G. Zhang, Y. Zhu, X. Wang, S.Dahl, I. Chorkendorf, *Angew. Chem. Int. Ed.*, 2013, **52**, 3621-3625.

[37] Y. Hou, A. B. Laursen, J. Zhang, G. Zhang, Y. Zhu, X. Wang, S.Dahl, I. Chorkendorf, *Angew. Chem. Int. Ed*., 2013, **52**, 3621-3625.

[38] K. G. Pradhan, K. M. Parida, *ACS Appl. Mater. Interfaces*, 2011, **3**, 317-323.

[39] G. K. Pradhan, D. K. Padhi, K. M. Parida, *ACS Appl. Mater. Interfaces,* 2013, **5**, 9101-9110.

[40] R. Li, Y. Jia, N. Bu, J.Wu, Q. Zhen, *J. Alloys Comp*. 2015, **643**, 88–93

[41] M.A. Ahmed, E. E. El-Katori, Z. H. Gharni, *J. Alloys Comp.* 2013, **553**, 19–29

[42] B. Palanisamy, C.M. Babu, B. Sundaravel , S. Anandan , V. Murugesan, *J. Hazard. Mater*. 2013, **252–253**, 233–242